Bio-Design and Manufacturing (2025) 8:511–523
https://doi.org/10.1631/bdm.2400372

RESEARCH ARTICLE

Magnetic nanoparticles for single-neuron manipulation to design a customized neural circuit

Hongyong Zhang[1,2] · Lingrui Zhao[3] · Nan Huang[1] · Xiaobo Zhang[3] · Tian Xu[3] · Sumin Bian[2] · Mohamad Sawan[2]

Received: 12 September 2024 / Accepted: 5 February 2025 / Published online: 22 May 2025

Abstract

The complexity and intricacy of the brain, which is composed of billions of neurons, pose significant challenges to its study. Understanding neural connections and communication at the single-cell level is crucial for unraveling the brain's functions. This study presents a novel strategy that utilizes magnetic nanoparticles (MNPs) and magnetic fields to manipulate neurons, thereby creating customized small-scale neural circuits for studying neural connections. To establish the feasibility of this approach, the effects of MNPs on neurons were initially investigated, demonstrating their low toxicity. Subsequently, a micromagnet array (MMA) chip was employed to manipulate the neurons, facilitating their precise arrangement on the electrodes. Over several days, the neurons extended their axons and established connections with neighboring cells, forming small-scale circular neural circuits. These artificially engineered circuits offer a simplified and controlled environment for studying neural networks in contrast to naturally occurring biological networks. Furthermore, electrophysiological recordings were conducted to investigate the connections between the manipulated neurons. This study introduces a customized small-scale neural circuit platform with electrode-specific recording and stimulating capabilities, enabling the study of neuron-to-neuron interactions at the single-cell level. By leveraging MNPs and an MMA chip, this research offers a powerful tool for studying neural connections and advancing our understanding of the brain's intricate workings.

Hongyong Zhang and Lingrui Zhao have contributed equally to this work.

✉ Sumin Bian
biansumin@westlake.edu.cn

✉ Mohamad Sawan
sawan@westlake.edu.cn

[1] Zhejiang University, Hangzhou 310027, China

[2] CenBRAIN Neurotech Center of Excellence, Westlake University, Hangzhou 310030, China

[3] Key Laboratory of Growth Regulation and Translational Research of Zhejiang Province, Hangzhou 310030, China

Graphical abstract

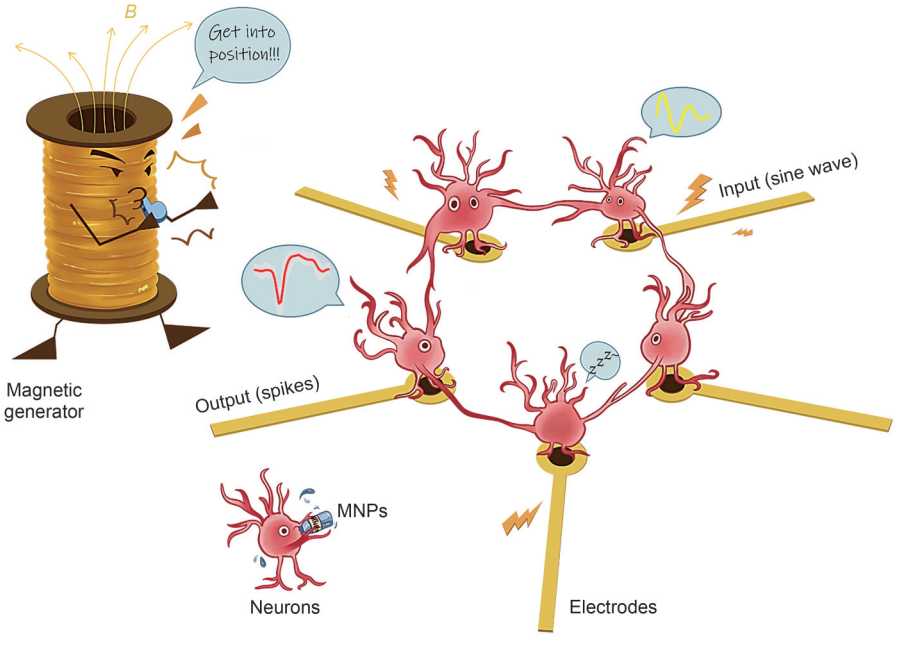

Keywords Single-cell manipulation · Neural circuits · Micromagnet array · Magnetic nanoparticles · Neural signal recording

1 Introduction

Understanding how individual neurons connect in the human brain is a challenging task due to the complexity of the brain and the limited microscopic technologies for in vivo studies [1]. However, advancements in bioengineering and electrophysiology have provided more reproducible methods for studying neural networks in vitro, offering insights into their fundamental characteristics and mechanisms [2, 3]. In vitro neural network models enable researchers to examine the intricate processes of neural circuit formation and neuron culture and observe their connectivity and activities under controlled conditions [4]. These models shed light on circuit assembly, synaptic pruning, and the establishment of functional connections. Notably, in the 1990s, in vitro circuits of three individual mollusk *Lymnaea* neurons demonstrated the simplest yet most sophisticated examples of in vitro single-neuron circuit functions [5]. Moreover, in vitro neural circuits provide a simplified and controlled environment for studying the fundamental principles of neural function [6]. In vitro neural circuits offer insights into information processing, the generation of action potential (AP) patterns, and their contributions to specific brain functions [7]. Research has shown that two-dimensional neural circuits with distinct segments and designated connections hold promise for analyzing network activities in vitro [8, 9].

In addition to advancing the understanding of neural networks, in vitro neural circuits have significant implications for modeling and studying neurological disorders [10]. Using patient-derived cells or organoids, researchers can recreate disease-specific circuitry and observe abnormal activity patterns or dysfunctions [11]. This approach provides an opportunity to investigate the mechanisms underlying developmental brain malfunctions, neurological damage, and neurodegenerative disorders. Various disease models, including Alzheimer's disease [12], Parkinson's disease [13], and amyotrophic lateral sclerosis [14], have been established using brain-organoid tissue cultures. Furthermore, in vitro neural circuits are crucial testing grounds for developing neuroprosthetic devices and brain–machine interfaces [15]. By interfacing with cultured neural circuits, researchers can explore the bidirectional communication between artificial devices and neurons, paving the way for advanced prosthetics, neural implants, and brain-controlled technologies [16]. Intriguingly, research has demonstrated that in vitro neural circuits can execute sequential game tasks, showcasing the ability of neural cultures to self-organize activities in a goal-directed manner and validating the "free energy principle" theory [17].

Despite the progress in neural network modeling in vitro, previous models have been limited in their ability to study the intricate details of neural connections due to their complexity

and randomness [18]. This study proposes a novel approach that focuses on single-cell studies, offering several advantages over traditional Petri dish cell cultures. Single-cell studies provide high-throughput capacity, simpler interaction models, and the potential to reveal individual differences [19]. Various techniques have emerged for manipulating cells, such as dielectrophoresis (DEP) [20], magnetic fields [21–23], acoustic waves [24], and on-chip microstructures [25]. Although DEP has been used to capture two types of cells in one microchamber for studying cell interactions, it is unsuitable for neurons because of the potential damage caused by electrical fields [26]. Magnetic fields combined with magnetic nanoparticles (MNPs) offer a promising avenue for single-cell manipulation due to the low toxicity to cells [27, 28]. Biocompatible MNPs [29], particularly iron oxide (FeO) nanoparticles with sizes on the order of tens of nanometers, have been extensively investigated in neuroscience for neuron labeling and imaging [30], neurite regeneration and guidance [31], and single-cell manipulation [32].

This study presents a novel approach for manipulating individual neurons on a micromagnet array (MMA) chip using magnetic fields. The magnetic manipulation system comprises a medium reservoir, an MMA chip, and a magnetic field generator (Fig. 1a). Each electrode captures an individual neuron, forming a specific-shaped neural circuit (Fig. 1b). Magnetic force and potential were utilized to induce MNPs into neurons, rendering them superparamagnetic and amenable to manipulation in a magnetic field (Fig. 1c). Neural signals were recorded from stimulated neurons as input and other neurons within the circuit as output using a neural signal recording system with a printed circuit board (PCB) adaptor (Fig. 1d). In addition, the interactions between neurons and MNPs were investigated by observing the responses of human stem-cell-induced cortical neurons to different types of MNPs. The effects on neuron viability, neuromorphology, and electrophysiology were assessed using both bovine serum albumin (BSA)-polyethylene glycol (PEG)-coated and uncoated MNPs. These findings have promising implications for the utilization of MNPs in neuron biology research and clinical treatments for brain disorders.

2 Materials and methods

2.1 Principle of cell manipulation based on the magnetic field

Figure 1c illustrates the principle of magnetized neurons driven by the magnetic field and captured by micromagnet electrodes. Normally, neural cells are not subjected to any force in a magnetic field. However, when cells are magnetized with MNPs, they have superparamagnetic properties and are subjected to a magnetic force F_{m} under the action of a magnetic field, as shown in Eq. (1):

$$F_{\mathrm{m}} = (m\nabla)B = \mu_0(m\nabla)H = \frac{1}{2}\mu_0\chi V\nabla H^2, \tag{1}$$

where B is the magnetic flux density, m is the magnetic moment of the cell, χ is the magnetic susceptibility of the cell, V is the volume of the cell, and $H = B/\mu_0$ is the magnetic field strength. Meanwhile, the cell has magnetic potential energy U_{m}, as shown in Eq. (2):

$$U_{\mathrm{m}} = -\mu_0 mH = -\frac{1}{2}\mu_0\chi VH^2. \tag{2}$$

Therefore, the cell is attracted to the cobalt (Co) electrode, where the local magnetic field strength is maximized and the magnetic potential energy is the lowest.

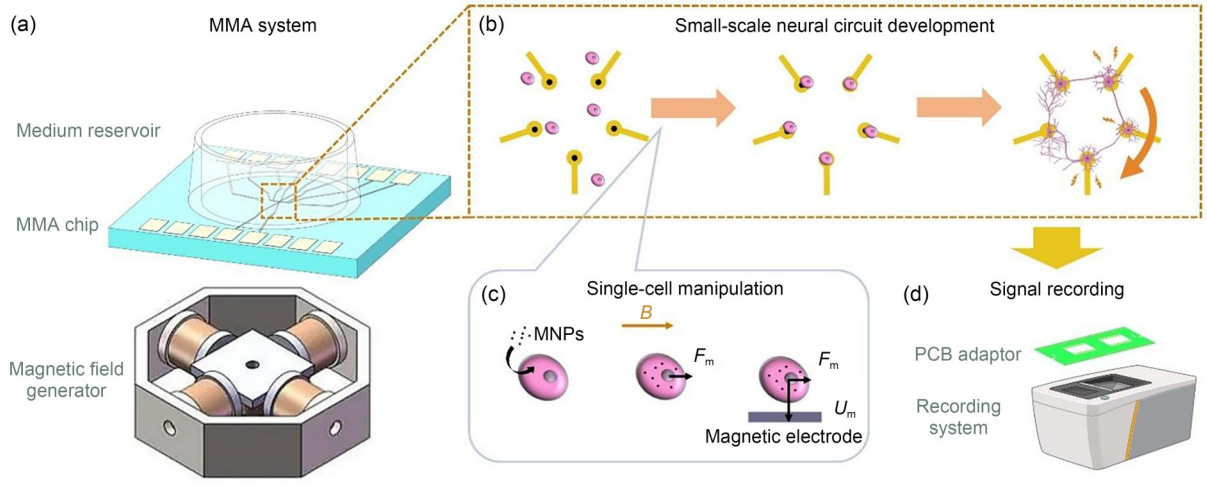

Fig. 1 Synthetic diagram of customized neural circuits using magnetic single-cell manipulation. (a) Components of the MMA system. (b) Process of building a specific-shaped neural circuit. (c) Principle of magnetic single-cell manipulation. (d) Neural signal recording by a commercial recording system with a PCB adaptor

2.2 MNP fabrication and characterization

The FeO cores were synthesized according to the methodology described in Ref. [33], resulting in nanoparticles with an average size of approximately 20 nm. The synthesis process involved the coprecipitation of ferrous (Fe^{2+}) and ferric (Fe^{3+}) ions in an alkaline solution. Specifically, 24.3 g $FeCl_3 \cdot 6H_2O$ and 16.7 g $FeSO_4 \cdot 7H_2O$ were dissolved in 200 mL deionized (DI) water under a nitrogen atmosphere and heated to 75 °C. Subsequently, a total of 45 mL of 25% (volume fraction) ammonia solution was gradually added to the vigorously stirred mixture. After 1 h reaction, the solution was cooled to room temperature, and the particles were collected using a magnet, washed with DI water five times, and dispersed in DI water.

To modify the nanoparticles with PEG, methoxy-PEG-silane with a molecular weight of 5000 was obtained from Nanoeast Biotech Co., Ltd. (Nanjing, China). MNPs were washed twice in ethanol, centrifuged, and dried at 110 °C for 1 h, followed by overnight vacuum-drying. Next, 15 mg of dried nanoparticles were dispersed in 5 mL toluene containing 3 mmol/L methoxy-PEG-silane. The mixture was vortex-mixed, sonicated, and incubated at 60 °C for 4 h. The resulting suspension was centrifuged, and the precipitates were sonicated in toluene for 10 min and washed with toluene and ethanol before vacuum-drying.

For the subsequent modification with BSA, a 1% (0.01 g/mL) BSA solution dissolved in phosphate-buffered saline (PBS) was prepared. This BSA solution was mixed with the nanoparticle solution at a volume ratio of 1:5 and vigorously stirred for 1 h at room temperature. To simulate the in vivo environment, the PEG-MNP and BSA-PEG-MNP suspensions were incubated in a 37 °C incubator for 1 week. Afterward, after drying at room temperature, the samples were dispersed on a copper grid for transmission electron microscopy (TEM) observation. PEG-MNPs agglomerated and adhered to each other after 1 week, whereas MNPs modified with BSA retained their individual, well-defined particle morphology. The average diameter of MNPs was approximately 20 nm, as measured using ImageJ.

2.3 Neural stem cell culture

Human neurons were derived from human-induced pluripotent stem cells (hiPSCs) using the neural induction protocol provided by STEMCELL Technologies (Shanghai, China). Initially, hiPSCs were induced into neural progenitor cells (NPCs) using the STEMdiff™ SMADi Neural Induction Kit (Catalog No. 08581). NPCs were then differentiated into neural cells using the STEMdiff™ Forebrain Neuron Differentiation Basal Medium (Catalog No. 08601). Neural maturation and functionality were induced using the STEMdiff™ Neuron Maturation Kit (Catalog No. 08510).

The iPSC line utilized in this study was commercially acquired from Sanqi Biological, Inc. (Shenzhen, China).

2.4 Immunostaining

For the fixation of neurons, 4% paraformaldehyde (PFA) was used to treat the cells for 10 min. Subsequently, the neurons were permeabilized using 0.3% Triton X-100 in PBS for 30 min. To prevent nonspecific binding, the cells were blocked overnight at 4 °C in a solution containing PBS with 3% BSA and 0.1% Triton X-100. For the incubation process, primary antibodies were added to the block solution, and the mixture was incubated at room temperature for 2 h. Similarly, secondary antibodies were subjected to the same conditions and incubated for 1 h. Lastly, to seal the coverslips, the stained sample was mounted with Fluoromount™ Aqueous Mounting Medium. In the experiment, microtubule associated protein 2 (MAP2, 1: 100; Cell Signaling Technology, USA) and TAU (1: 1000; Cell Signaling Technology) were utilized as specific markers for the neurons. Additionally, 4′,6-diamidino-2-phenylindole (DAPI; 1: 500; Invitrogen, USA) was applied as a standard marker for cell nuclei.

2.5 Neuron manipulation with a magnetic field

A desktop magnetic field generator was custom-designed and purchased from Tinduan Industry (Shanghai, China), which could be placed under the microscope (Fig. S1 in the supplementary information). It contained five electromagnets, two in the *x*-direction, two in the *y*-direction, and one in the *z*-direction, which could be controlled independently. The accompanying current source was used to apply the current. The actual magnetic field in the chip area was measured and calibrated every time before the experiments using a magnetic flux meter. To prevent neural deposition on the ground electrodes, which would disturb the signal recording, small droplets (approximately 20 μL) of the neuron-MNP combination were first dripped on the working electrode area. Then, the magnetic field was applied to manipulate the cells by generating external forces from different directions to trigger neuron movements, pushing them to settle onto the designated electrodes and adhere for 24 h at 37 °C. The corresponding culture media were then added.

2.6 Fabrication of the MMA chip

The MMA chip was fabricated by standard lithography and the lift-off technique (Fig. S2a in the supplementary information). Briefly, a layer of photoresist AZ1518 (Merck, Germany) was spin-coated on the indium tin oxide (ITO) glass and patterned by lithography. An acid solution containing 16% (volume fraction) HCl and 3% (volume fraction) HNO_3 was used to etch the ITO. The excess photoresist was

removed using acetone. Another layer of the photoresist was patterned using the same steps. A layer of 100 nm Co was added, and the redundant Co was removed with acetone to complete the lift-off step. Finally, a thin photoresist was patterned using the same steps as the insulating layer.

The medium reservoir was fabricated using a reverse mold of polydimethylsiloxane (PDMS) (Fig. S2b in the supplementary information). A cylindrical void mold was designed and fabricated by a three-dimensional printer, and PDMS was poured into the mold. After overnight curing, the PDMS was demolded to obtain the reservoir. The MMA chip and reservoir were cleaned by plasma treatment simultaneously and gently fixed together.

2.7 Fabrication and characterization of poly (3,4-ethylenedioxythiophene)-poly (styrenesulfonate) (PEDOT:PSS) coatings

To coat the microelectrodes, the standard electroplating process was employed, which can be summarized as follows: (1) Preparation of the PEDOT:PSS electrolyte: A mixture of 20 mmol/L PEDOT (Klamar, Shanghai, China) and PSS (Klamar) at 0.4% (4 g/L) was prepared in DI water. (2) Cleaning the MMA chip: The MMA chip was cleaned using acetone, followed by oxygen plasma treatment to ensure a clean surface. (3) Connection of microelectrode pads: Platinum (Pt) wires were connected to the microelectrode pads using conducting resin, establishing electrical contact. (4) Electroplating setup: The working electrode (Pt) was attached to the cathode, and the sample to be coated was connected to the anode for electroplating. (5) Deposition of PEDOT:PSS: PEDOT:PSS deposition was carried out for 10 min at 2 V. Note that the voltage should not exceed 3 V to prevent delamination of the ITO electrodes. To assess the impedance of the microelectrodes before and after PEDOT:PSS coating, an Intan RHX recording and stimulation system (Intan Technologies, Los Angeles, CA, USA) was used. The electrodes were immersed in 1× PBS solution, and the impedance measurements were performed at 1 kHz.

2.8 Neural viability, neuromorphology, and electrophysiology monitoring

Neural viability was assessed using a commercially available calcein acetoxymethyl ester (calcein-AM)/propidium iodide (PI) staining kit (Solarbio, Beijing, China). The following procedure was employed: First, the culture medium was carefully aspirated, and the neurons were gently washed with PBS thrice. Subsequently, a staining solution was prepared and added to the culture dish. The neurons were incubated at 37 °C for 15 min and observed under a fluorescence microscope. The resulting data were quantified using ImageJ and manually verified.

To monitor the neuromorphology of neurons over an extended period, the Incucyte Live-Cell Analysis System (Sartorius, Göttingen, Germany) was utilized. Neurons were cultured within the system, with or without nanoparticles, and imaged at 30-min intervals. The Incucyte equipment captured images of the neurons and the corresponding neurites and somas. The accompanying software facilitated the data collection and analysis of the neurite length and soma characteristics.

For recording and analyzing neural activity, the Axion Maestro Pro system (Axion BioSystems, Atlanta, GA, USA), a commercial neural signal recording system, was employed. Neurons were cultured on a custom-designed microelectrode array (MEA) 24-well plate, which included 16 electrodes per well. This MEA plate was inserted into the Axion system, enabling the capture and analysis of various neural events, such as spikes and bursts.

2.9 TEM imaging

For TEM imaging, the neuron samples were fixed with 2% glutaraldehyde and 2% PFA in 0.1 mol/L sodium cacodylate buffer for 30 min and washed in ice-cold 0.1 mol/L sodium cacodylate buffer thrice. Next, cells were postfixed in reduced 1% osmium tetroxide in cacodylate buffer for 1 h and rinsed with 0.1 mol/L sodium cacodylate buffer thrice. After washing with DI water thrice, cells were stained with 1% uranyl acetate in DI water for 1 h. Next, cells were rinsed with DI water, dehydrated with a graded ethanol series, and infiltrated with Durcupan ACM resin. Finally, ultrathin sections were prepared, and TEM images were acquired with TEM (Talos L120C G2; Thermo Scientific, Massachusetts, USA) at 120 kV.

2.10 Scanning electron microscopy (SEM) imaging

To prepare the SEM sample for analysis, the following steps were undertaken: Neurons were initially fixed in a solution containing 2.5% glutaraldehyde and 2% PFA obtained from Yuanye Biotechnology (Shanghai, China). The fixation process was carried out at 4 °C for 1 h. The fixed sample was washed thrice using 0.1 mol/L phosphate buffer (PB) at pH 7.3 to remove any excess fixative. Subsequently, the neurons underwent a secondary fixation by immersing them in 1% osmium tetroxide (dissolved in 0.1 mol/L PB) on ice for 1 h. After the secondary fixation, the sample was gently washed thrice with DI water to eliminate the residual osmic acid. To facilitate SEM analysis, the sample was dehydrated using a gradient of alcohol concentrations, beginning with 30% alcohol and gradually increasing to 95%. This was followed by three subsequent dehydration steps using 100% alcohol. To ensure complete dryness, the dehydrated

sample was subjected to a critical point drying process, which involved replacing the alcohol with a suitable drying medium while preserving the sample's structure. Finally, a thin layer of gold (approximately 5 nm thick) was deposited onto the sample surface. This gold coating served to enhance the sample's conductivity and optimize imaging during SEM analysis.

2.11 Energy-dispersive spectrometry (EDS) analysis

EDS is an advanced microbeam analytical technique that meticulously identifies and quantifies the elemental composition within a sample. This process is accomplished by meticulously measuring the X-ray energies emanating from the interaction between an electron beam and the sample material, thereby unraveling the type and content of the constituent elements. In the context of MNP analysis, a simple sample preparation protocol was adopted. Specifically, a 20 μL droplet, containing 20 μg/mL MNPs, was dispersed onto a silicon (Si) wafer. This assembly was subsequently subjected to a thermal treatment at 40 °C for 30 min, facilitating the evaporation of the solvent and ensuring a stable, dried sample for analysis. To further enhance the electrical conductivity of the surface, a uniform layer of 5 nm Pt was carefully deposited, fostering optimal conditions for subsequent analysis. The prepared sample was initially visualized under SEM, enabling the selection of a region densely populated with MNPs. This region was subjected to rigorous examination using the EDS probe, which provided a comprehensive elemental fingerprint of MNPs.

2.12 Acquisition and analysis of neural signals

The connectivity between the MMA chip in this study and the commercial system was established using a custom-designed PCB. This PCB facilitated the seamless integration and communication between the MMA chip and the commercial system. Data acquisition was performed using the neural spike setting, employing a gain of 1000× and a bandpass filter from 0.2 to 4.0 kHz. These settings ensured optimal signal capture and reduced noise interference during data collection. For spike detection and analysis, the AxIS software was employed. The spikes were identified as signals with amplitudes exceeding a threshold of 6 standard deviations (SDs) from the mean noise level. In contrast, bursts were defined as a minimum of five consecutive spikes with a maximum interspike interval of 100 ms. By implementing these methodologies, the connection between the MMA chip and the commercial system was effectively established, enabling precise data collection and analysis.

3 Results

3.1 Characterization of MNPs and neurons

MNPs were synthesized using the coprecipitation method as described above. To improve the long-term dispersion and reduce potential neurotoxicity, MNPs were coated with PEG and BSA. The morphology of uncoated MNPs was observed using TEM (Fig. 2a), and the dispersion of the particles is depicted in Fig. 2b. Results showed that these nanoparticles had a uniform shape, good dispersion, and a particle size of approximately 20 nm. To further examine the composition of these particles, a combination of SEM and EDS analyses was employed. This technique was used to examine the types and elemental composition within the microregion of MNP-treated neurons, as depicted in Fig. 2c. Due to the sample preparation steps, some impurities were introduced during sample preparation, such as Pt (coating material) and Si (substrate), resulting in a decreased mass fraction of Fe and O. The atomic number ratio could be calculated from the results, which is Fe:O=3:4.3, indicating the structure of the nanoparticles.

The attainment of neural maturity and functionality holds paramount significance in the intricate process of neural network formation and signaling. Emerging evidence from various studies underscores the intellectual prowess and heightened activity exhibited by human nerve cells compared to their murine counterparts [17]. To enhance the construction of sophisticated neural networks, a pioneering approach was undertaken to derive human neurons from hiPSCs, thereby harnessing the unique capabilities of the human neural lineage. The successful maturation of these neurons was meticulously validated through immunostaining procedures targeting key markers such as TAU, DAPI, and MAP2, as depicted in Fig. 2d.

3.2 Interaction between MNPs and neurons

Before manipulating neurons with magnetic fields, it is necessary to magnetize the neurons using MNPs. The effects of these MNPs on neurons were studied using SEM to observe the surface of neurons treated with 20 μg/mL MNPs and untreated neurons (Figs. 3a and 3b). Neurons exposed to MNPs exhibited an increased presence of the secreted material on their surfaces compared to normal cultured neurons, suggesting that adding MNPs may stimulate the secretion of exosomes in neurons. Furthermore, TEM was employed to examine the cross-sections of the neurons, revealing the internal presence of MNPs within the vesicles (Fig. 3c), indicating that MNPs were not only absorbed on the surface of the neurons but also internalized by living neurons. To quantify the presence of MNPs within the neurons, a square area was selected and further analyzed by EDS, as shown in

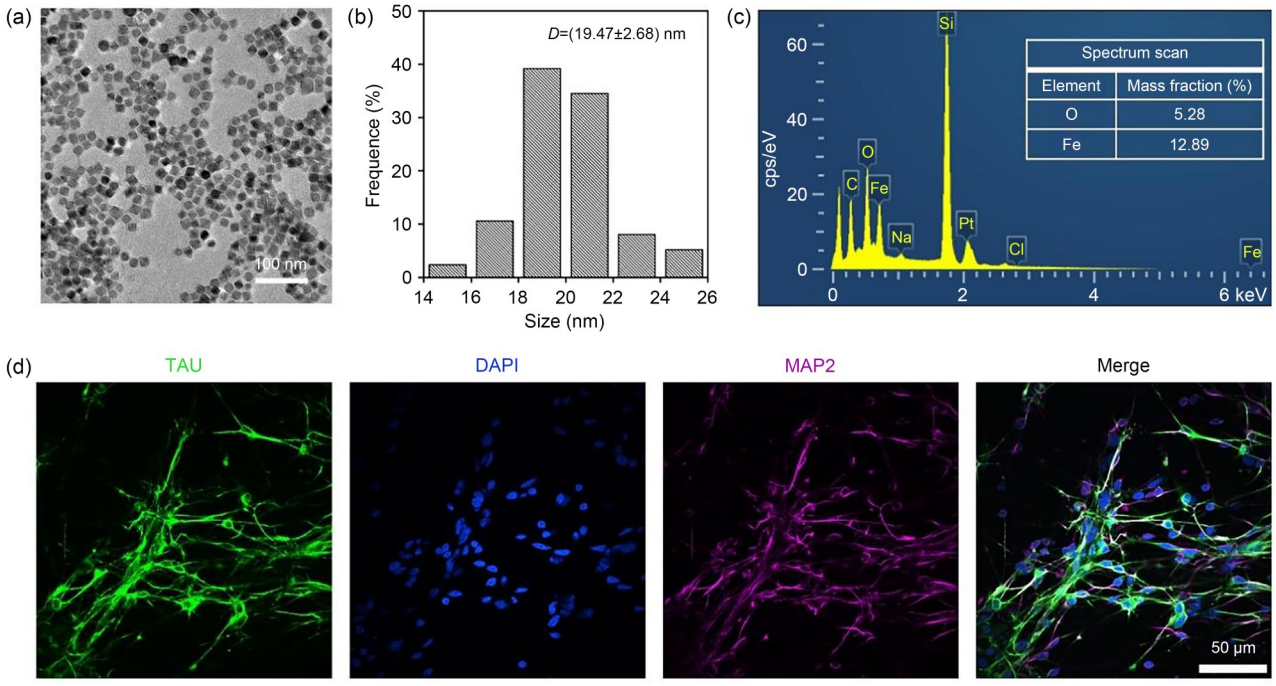

Fig. 2 Characterization of MNPs and neurons. (a) TEM imaging of synthesized MNPs. (b) Statistical diameter results of MNPs, demonstrating that the average diameter is 19.47 nm, with a uniform shape and good dispersion. (c) EDS analysis results of MNPs for element validation. The mass fractions of Fe and O are 12.89% and 5.28%, respectively, demonstrating that the atomic number ratio is 3∶4.3. (d) Immunostaining of neurons with TAU, DAPI, and MAP2 to demonstrate their maturation

Figs. 3d and 3e. Results revealed a mass fraction of 2.09% for Fe, providing further evidence of successful MNP endocytosis in neurons.

Next, a comprehensive study was conducted to assess the influence of MNPs on neurons in terms of viability, neuromorphology, and electrophysiology. Neural viability was evaluated 24 h after the addition of MNPs using the calcein-AM/PI staining kit as described above, as shown in Fig. S3 (supplementary information). Neurons cultured without MNPs exhibited viability of >90% in the control group, as illustrated in Fig. 4a. However, the addition of 10 μg/mL uncoated MNPs resulted in significant damage to the neurons, reducing their viability to <30% rapidly. In contrast, using BSA-PEG-coated MNPs, neural viability increased significantly, indicating the favorable biocompatibility of these modified MNPs. To examine the effect of MNPs on neurites, the average neurite length per cell body was evaluated using the Incucyte Live-Cell Analysis System (Fig. S4 in the supplementary information). Specifically, somas were represented by pink dots, whereas neurites were depicted as yellow lines. Considering the balance between neural viability and manipulation efficiency, a concentration of 20 μg/mL was used. Neurons treated with BSA-PEG-coated MNPs exhibited a decrease in the average neurite length per cell body compared to untreated neurons (control group) (Fig. 4b), indicating an impairment in neural morphological development. However, within subsequent hours, the neurites displayed renewed extension, similar to the control group, suggesting that the side effects are relatively minor.

To monitor neural activity, neurons were monitored using a signal recording system for 30 min every 3 d. Spike rates were counted to demonstrate the neural activity, which commenced on day in vitro (DIV) 12 and reached its peak around DIV 27 (Fig. 4c). Figure 4d displays fragments of the original signals from neurons, untreated (left) and treated with MNPs, on DIV 27. The accompanying software was utilized to detect spikes and bursts, defining spikes as signals exceeding 6 SDs of the mean noise level and bursts as a minimum of 5 spikes with a maximum interspike interval of 100 ms. The raster plot of spikes in Fig. 4e demonstrates the recording of spontaneous activity in neurons treated with different types of MNPs during a 1-min interval on DIV 27. The addition of BSA-PEG-coated MNPs only slightly decreased the neural activity, indicating the low neurotoxicity of these MNPs. To assess the long-term stability of the coated MNPs within neurons and in biological media, a 24-h culture of neurons with MNPs was followed by regular fresh medium changes every 2 d for 2 weeks. Subsequently, the neurons were dissociated and disrupted by suspension in water under vigorous vibration. The resulting solution was thoroughly mixed, and a droplet was placed on a copper wire mesh for TEM observation, as illustrated in Fig. S5 (supplementary information). Although some organic matter was observed to be attached, the shape of MNPs

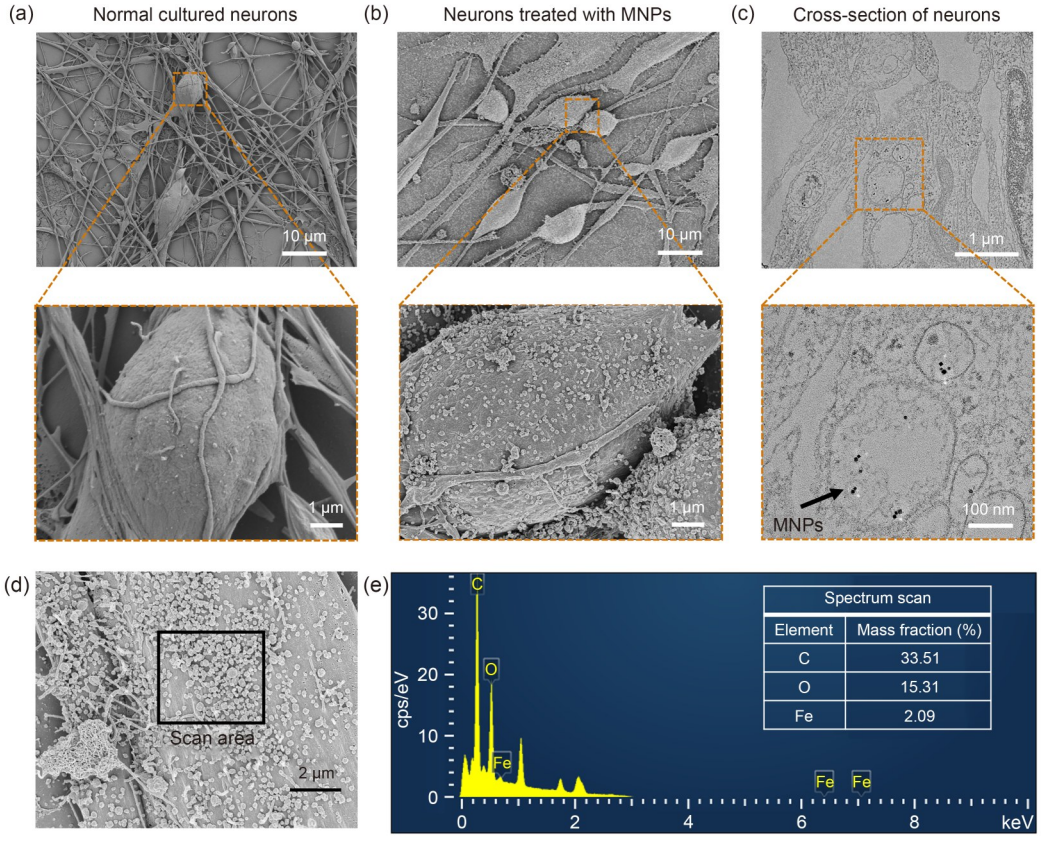

Fig. 3 Interaction between MNPs and neurons. (a) SEM imaging of normal cultured neurons, showing the smooth surface of neurons. (b) Neurons treated with MNPs by SEM, showing a great increase in secreted exosomes. (c) Cross-section of neurons treated with MNPs by TEM, showing the existence of vesicles containing MNPs. (d) SEM image of neurons with MNPs, where the area in the black frame was selected and scanned by EDS, to quantitatively analyze MNPs in neurons. (e) EDS results of the selected area in (d), showing that the mass fraction of Fe is 2.09%

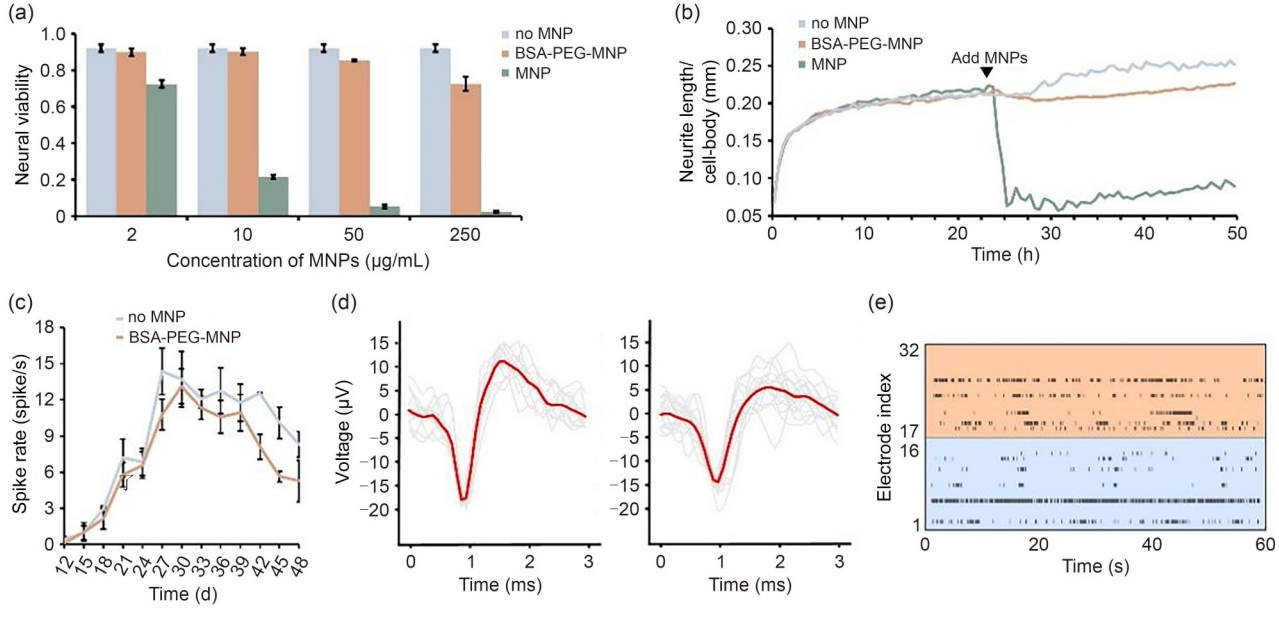

Fig. 4 Influence of MNPs on neurons. (a) Statistical results of neural viability after 24 h addition of MNPs. (b) Neural morphological study by calculating neurite length per cell body. MNPs were added at 24 h at 20 μg/mL. (c) Electrophysiological study of neurons treated and untreated with MNPs by recording the spike rate every 3 d. (d) Fragments of original signals from neurons, untreated (left) and treated (right) with MNPs, on DIV 27. (e) Raster plot of spikes from neurons, untreated (electrodes 1–16) and treated (electrodes 17–32) with MNPs, on DIV 27. Data in (a, c) are expressed as mean±standard deviation (n=5)

remained clear and stable, indicating their enduring stability within neurons over an extended period.

3.3 Cell manipulation on the MMA chip

Figure 5a shows the microelectrode-MMA design, where the working electrodes are aligned with the ground electrode in proximity (Fig. S6 in the supplementary information). The MMA comprises eight ITO electrodes, each featuring a central micromagnet. The ITO electrodes serve for neural recording, whereas the Co electrodes enable cell manipulation. To enhance the electrode biocompatibility and reduce the impedance, a surface coating of PEDOT:PSS was employed (Fig. 5b). This coating resulted in a decrease in the electrode impedance from about 57.8 kΩ to about 10 kΩ, which was sustained for >2 weeks (Fig. 5c; Fig. S7 in the supplementary information). Additionally, the microelectrodes were magnetized by placing the chip on a 4-kG (1 G= 0.0001 T) permanent magnet overnight. Subsequently, a PDMS medium reservoir was bonded to the MMA after plasma treatment, and neurons containing MNPs were introduced into the reservoir. The device was then positioned on a magnetic field generator, where the neurons were manipulated by the magnetic field. The entire device and operation process were observed under a microscope (Olympus, Japan), as depicted in Fig. S8 (supplementary information). To prevent the demagnetization of the micromagnets, the applied field strength was kept at <100 G. To determine the optimal concentration for neural manipulation, the neurons were subjected to a horizontal magnetic field of 100 G. As the concentration of MNP treatment increased, the speed of neural movement also increased, as demonstrated in Fig. 5d. Cells treated with the same MNP concentration exhibited variable speeds based on the number of attached MNPs. Consequently, the error bars in the data were substantial. Neurons that appeared slightly darker possessed more attached MNPs and exhibited greater mobility. To balance cell viability and manipulation efficiency, 20 μg/mL MNPs were determined and utilized in subsequent experiments.

To identify the optimal magnetic field parameters, various field strengths and angles were explored using high-density MMAs (Fig. 5e). The capture efficiency, defined as the total number of captured cells divided by the total number of cells present 30 s after applying the magnetic field, was evaluated

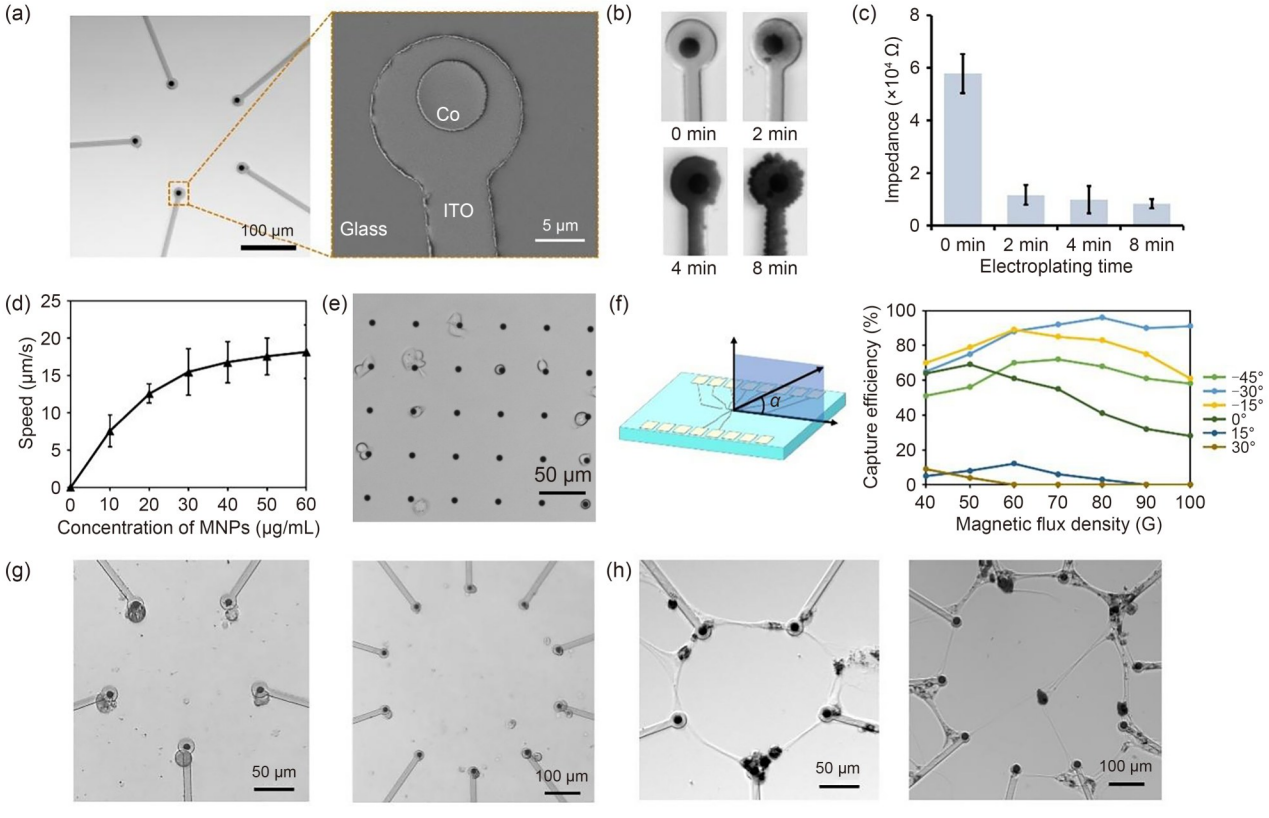

Fig. 5 MMA chip fabrication and single-cell manipulation. (a) MMA electrode design imaged by optical microscopy (left) and SEM (right). (b) Electroplating of PEDOT:PSS on electrodes with different electroplating times. (c) Decrease of electrode impedance after PEDOT:PSS coating with different electroplating times. (d) Speed of neural movement under 100 G magnetic field, with different concentrations of MNP treatments. (e) Neural manipulation test on high-density MMAs for pilot study to find the best parameter for cell manipulation. (f) Capture efficiency under different angles and amplitudes of magnetic flux density. (g) Single-cell manipulation on two different MMAs. (h) Establishment of two different neural circuits on MMA. 1 G=0.0001 T. Data in (c, d) are expressed as mean±standard deviation (n=5)

(Fig. 5f). Based on these data, the optimal replenishment parameters were found to be approximately 70 G with a − 30° angle. Excessive magnetic field strength that led to rapid cell movement could result in replenishment failure. However, a negative angle allowed the cells to slide or roll along the underside of the chip, facilitating capture, whereas a positive angle pulled the cells away from the electrode. The specific optimal parameters depended on factors such as cell size, magnetization, and environmental conditions, and required minor adjustments. Once all electrodes successfully captured an individual cell, the horizontal magnetic field was removed, leaving only the vertical magnetic field, and the cell adhered to the wall for 5 min to strengthen the connection (Fig. 5g). Subsequently, the chips were slowly placed in the incubator and left undisturbed for 1 h, and 1 mL culture medium was gradually added along the tank wall. After a few days of culturing, the cells established connections with each other, forming neural circuits, as depicted in Fig. 5h. Due to cell migration, some cell bodies exhibited slight displacement from the electrodes.

3.4 Neural activity recording

Conductive silver glue was employed to establish the connection between the MMA chip and the custom-designed PCB, which facilitated the recording of electrical signals using the instrument, as illustrated in Fig. S9 (supplementary information). The PCB had the capacity to accommodate two chips simultaneously, thereby enhancing the efficiency of neural recording. To ensure the reliable formation of neural circuits, stimulation was performed at different positions within the circuit while APs were recorded from DIV 18 to 27. In the absence of stimulation, spontaneous axonal signal propagation was scarcely detectable. This could be attributed to the differentiation and culture conditions of stem cell-induced forebrain neurons [34] and the sparse distribution of individual neurons, which might contribute to the absence of spontaneous APs.

Mild stimulation was conducted at electrode 1 (Fig. 6a), and AP propagation was recorded at electrodes 2 and 3. The average peak-to-peak amplitude of the triggered APs was 25 and 19 μV at electrodes 2 and 3, respectively. Because the presence of stimulated spikes can serve as a criterion for neural activity [15], stimulation was also introduced at the other two electrodes. When stimulation was applied at electrode 2 (Fig. 6b), the average peak-to-peak amplitude of the triggered APs was 25 and 22 μV at electrodes 1 and 3, respectively. Similarly, when stimulation was introduced at electrode 3 (Fig. 6c), the average peak-to-peak amplitude of the triggered APs was 27 and 22 μV at electrodes 1 and 2, respectively. Notably, minimal time lapses were observed among the three APs of the neurons, regardless of the position of the stimulation, suggesting that individual neurons establish physical and functional junctions, exhibiting responsiveness to stimulation and efficient AP propagation.

4 Discussion

In this study, magnetically driven MNPs were employed to manipulate individual neurons, demonstrating their potential for morphological and functional connectivity. The magnetic microrobot manipulation system utilized in this study offered advantages such as reproducibility, low cytotoxicity, and high accuracy in neural connection. Building upon the previous study that utilized electric fields for cell manipulation and yielded similar results [26], the magnetic microrobot manipulation system was designed and optimized in this study, including biotechnology parameters such as biocompatible coatings for magnetic beads and rearrangement of electrode arrays on the chip. These optimizations aimed to enhance neural connections. To improve the biocompatibility of the magnetic microrobots in neuron analysis, Fe_3O_4 nanoparticles were coated with dual coatings of BSA and PEG. This approach not only improved dispersion in the cell culture medium but also increased biocompatibility and reduced cytotoxicity. Using this method, individual neurons were successfully manipulated while preserving their neural morphology, cell viability, and electrophysiological functions. These findings indicated that neurons in an MNP solution retained their viability but showed susceptibility to MNPs, highlighting potential side effects that should be considered in the clinical use of MNPs in therapies. This technique differs from single-cell isolation or microinjector methods, as it can be directly performed in the cell culture environment with a shorter operation time window. By coculturing with neurons, the magnetic microrobots can be wirelessly controlled using an external magnetic field, eliminating the exposure of cells and culture medium to the external atmosphere and significantly improving cell viability.

The proposed MNP manipulation system holds promise as a reliable and safer tool for designing in vitro neural circuits. Using specifically designed chip electrodes and circuits, it is possible to establish specific neural circuits and enable the formation and connection of individual neural processes [35]. The control system for the magnetic field, as an integral part of the robotic system, plays a crucial role in the precise manipulation of nanosized microrobots and the formation of single-neuron connections or artificial neural networks (ANNs). Future research should evaluate whether next-generation magnetic microrobots can directly screen and connect cells based on biochemical factors such as neural types (e.g., neurons expressing specific receptors or antibodies) and cell viability. Additionally, determining the optimal intensity of the external magnetic field will be crucial for achieving stability in neural networks.

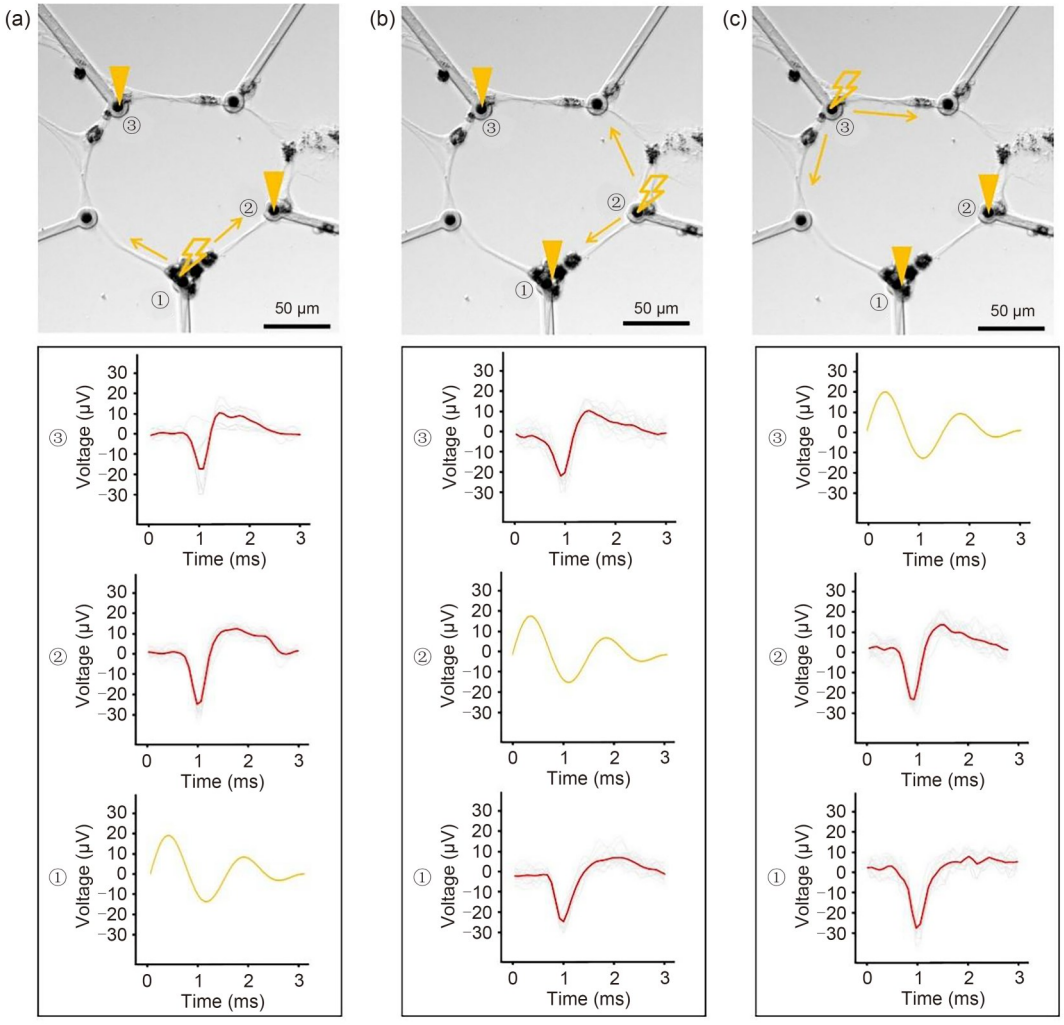

Fig. 6 Electrophysiological stimulation and recording of the neural circuit. (a) Stimulate electrode 1 and record at electrodes 2 and 3. (b) Stimulate electrode 2 and record at electrodes 1 and 3. (c) Stimulate electrode 3 and record at electrodes 1 and 2

The limitations of Si chips, including high energy consumption and heating issues, have prompted researchers to seek alternative computing approaches. By replacing electronic components with neurons, the computational capabilities of the chips can be significantly enhanced. Neurons offer inherent parallel processing abilities, enabling the simultaneous analysis of multiple inputs and rapid decision-making. Inspired by the brain's resource allocation mechanisms, neurons' energy-efficient operation holds promise for reducing power consumption and heat generation. However, integrating neurons into the chip design presents challenges, including developing effective interfaces, ensuring long-term stability, and optimizing scalability. Overcoming these hurdles will pave the way for the realization of highly efficient and powerful neuron-based computing devices, revolutionizing the field of computation.

Although the electrophysiological signals detected in this study are relatively weak, several limitations may have influenced the recording of neural activity signals on the MMA. The sparse density of cultured neurons after using magnetically driven MNPs to manipulate individual neurons may have hindered the recording of spontaneous APs. Shortening the operation time window and optimizing the culture medium (e.g., by adding potassium ions) may improve AP signals. The spontaneous shifting of neurons tethered to the electrodes could also lead to inaccurate electrophysiological recordings. Furthermore, differences in the electrode quality and impedance may result in varying response levels of the cells [36].

Although iPSC-derived neurons were used in this study, future investigations should focus on manipulating primary neurons, as previous studies have successfully manipulated primary neurons such as olfactory receptor neurons [37] and rat hippocampus primary neurons [38]. This method opens possibilities for single-cell neuron manipulation and electrophysiological detection, serving as a potential foundation for advanced controllable in vitro ANN models. Moreover, introducing controllable magnetic nanoscale microrobots may enable the reconstruction of more complex

ANNs. With input and output, researchers can even accomplish simple functions by training the neural networks. The authors envision that this magnetic microrobot manipulation system can be applied in other research fields, involving tumor cell migration/invasion studies, organoid-derived drug screening, and precision-medicine platforms.

Supplementary Information The online version contains supplementary material available at https://doi.org/10.1631/bdm.2400372.

Acknowledgements This research was supported by Westlake University and the Research Center for Industries of the Future of Westlake University (No. WU2022C040).

Author contributions HYZ, LRZ, TX, and MS conceived the overall research goals and aims. HYZ and SMB performed the designs, engineering investigation, and manufacturing for the devices. HYZ, LRZ, and XBZ were responsible for electrophysiological data collection and analysis. HYZ, LRZ, and NH conducted the statistical analyses and performed live-cell imaging experiments and analysis. HYZ and LRZ were responsible for the original drafting of the manuscript. All authors assisted in critical editing and review of the final manuscript.

Declarations

Conflict of interest The authors declare that they have no competing financial interests or personal relationships that could have appeared to influence the work reported in this paper.

Ethical approval This article does not contain any studies with human or animal subjects performed by any of the authors.

Data availability The datasets used during the current study are available from the corresponding authors upon reasonable request.

References

1. Pasca SP (2018) The rise of three-dimensional human brain cultures. Nature 553(7689):437–445. https://doi.org/10.1038/nature25032
2. Gupta P, Shinde A, Illath K et al (2022) Microfluidic platforms for single neuron analysis. Mater Today Bio 13:100222. https://doi.org/10.1016/j.mtbio.2022.100222
3. Sheng WQ, Li Y, Qin CL et al (2024) Integrated nanoporous electroporation and sensing electrode array for total dynamic time-domain cardiomyocyte membrane resealing assessment. Bio-Des Manuf 7(6):972–982. https://doi.org/10.1007/s42242-024-00308-z
4. Tsai D, Sawyer D, Bradd A et al (2017) A very large-scale microelectrode array for cellular-resolution electrophysiology. Nat Commun 8(1):1802. https://doi.org/10.1038/s41467-017-02009-x
5. Syed NI, Bulloch AG, Lukowiak K (1990) In vitro reconstruction of the respiratory central pattern generator of the mollusk *Lymnaea*. Science 250(4978):282–285. https://doi.org/10.1126/science.2218532
6. Huang Q, Tang BH, Romero JC et al (2022) Shell microelectrode arrays (MEAs) for brain organoids. Sci Adv 8(33):eabq5031. https://doi.org/10.1126/sciadv.abq5031
7. Pelkonen A, Mzezewa R, Sukki L et al (2020) A modular brain-on-a-chip for modelling epileptic seizures with functionally connected human neuronal networks. Biosens Bioelectron 168:112553. https://doi.org/10.1016/j.bios.2020.112553
8. Buccelli S, Bornat Y, Colombi I et al (2019) A neuromorphic prosthesis to restore communication in neuronal networks. iScience 19:402–414. https://doi.org/10.1016/j.isci.2019.07.046
9. Yamamoto H, Moriya S, Ide K et al (2018) Impact of modular organization on dynamical richness in cortical networks. Sci Adv 4(11):eaau4914. https://doi.org/10.1126/sciadv.aau4914
10. Kajtez J, Buchmann S, Vasudevan S et al (2020) 3D-printed soft lithography for complex compartmentalized microfluidic neural devices. Adv Sci 7(16):2001150. https://doi.org/10.1002/advs.202001150
11. Harberts J, Siegmund M, Schnelle M et al (2021) Robust neuronal differentiation of human iPSC-derived neural progenitor cells cultured on densely-spaced spiky silicon nanowire arrays. Sci Rep 11(1):18819. https://doi.org/10.1038/s41598-021-97820-4
12. Zhao J, Fu Y, Yamazaki Y et al (2020) APOE4 exacerbates synapse loss and neurodegeneration in Alzheimer's disease patient iPSC-derived cerebral organoids. Nat Commun 11(1):5540. https://doi.org/10.1038/s41467-020-19264-0
13. Zagare A, Barmpa K, Smajic S et al (2022) Midbrain organoids mimic early embryonic neurodevelopment and recapitulate LRRK2-p.Gly2019Ser-associated gene expression. Am J Hum Genet 109(2):311–327. https://doi.org/10.1016/j.ajhg.2021.12.009
14. Kemmerer ZA, Robinson KP, Schmitz JM et al (2021) UbiB proteins regulate cellular CoQ distribution in *Saccharomyces cerevisiae*. Nat Commun 12:4769. https://doi.org/10.1038/s41467-021-25084-7
15. Gao K, Gao F, Li J et al (2021) Biomimetic integrated olfactory sensory and olfactory bulb systems in vitro based on a chip. Biosens Bioelectron 171:112739. https://doi.org/10.1016/j.bios.2020.112739
16. Cai HW, Ao Z, Tian CH et al (2023) Brain organoid reservoir computing for artificial intelligence. Nat Electron 6(12):1032–1039. https://doi.org/10.1038/s41928-023-01069-w
17. Kagan BJ, Kitchen AC, Tran NT et al (2022) In vitro neurons learn and exhibit sentience when embodied in a simulated game-world. Neuron 110(23):3952–3969.e8. https://doi.org/10.1016/j.neuron.2022.09.001
18. Abbott J, Ye TY, Krenek K et al (2020) A nanoelectrode array for obtaining intracellular recordings from thousands of connected neurons. Nat Biomed Eng 4(2):232–241. https://doi.org/10.1038/s41551-019-0455-7
19. Luo T, Fan L, Zhu R et al (2019) Microfluidic single-cell manipulation and analysis: methods and applications. Micromachines 10(2):E104. https://doi.org/10.3390/mi10020104
20. Farasat M, Chavoshi SM, Bakhshi A et al (2022) A dielectrophoresis-based microfluidic chip for trapping circulating tumor cells using a porous membrane. J Micromech Microeng

32(1):015008.
https://doi.org/10.1088/1361-6439/ac3c89
21. Rampini S, Kilinc D, Li P et al (2015) Micromagnet arrays for on-chip focusing, switching, and separation of superparamagnetic beads and single cells. Lab Chip 15(16):3370–3379.
https://doi.org/10.1039/c5lc00581g
22. Lee H, Liu Y, Ham D et al (2007) Integrated cell manipulation system—CMOS/microfluidic hybrid. Lab Chip 7(3):331–337.
https://doi.org/10.1039/b700373k
23. Lee H, Liu Y, Westervelt RM et al (2006) IC/Microfluidic hybrid system for magnetic manipulation of biological cells. IEEE J Solid State Circ 41(6):1471–1480.
https://doi.org/10.1109/JSSC.2006.874331
24. Yang Y, Pang W, Zhang H et al (2022) Manipulation of single cells via a stereo acoustic streaming tunnel (SteAST). Microsyst Nanoeng 8:88.
https://doi.org/10.1038/s41378-022-00424-9
25. Habibey R, Rojo Arias JE, Striebel J et al (2022) Microfluidics for neuronal cell and circuit engineering. Chem Rev 122(18): 14842–14880.
https://doi.org/10.1021/acs.chemrev.2c00212
26. Zhang HY, Wang PB, Huang N et al (2023) Single neurons on microelectrode array chip: manipulation and analyses. Front Bioeng Biotechnol 11:1258626.
https://doi.org/10.3389/fbioe.2023.1258626
27. Socoliuc V, Peddis D, Petrenko VI et al (2020) Magnetic nanoparticle systems for nanomedicine: a materials science perspective. Magnetochemistry 6(1):2.
https://doi.org/10.3390/magnetochemistry6010002
28. Levada K, Pshenichnikov S, Omelyanchik A et al (2020) Progressive lysosomal membrane permeabilization induced by iron oxide nanoparticles drives hepatic cell autophagy and apoptosis. Nano Converg 7(1):17.
https://doi.org/10.1186/s40580-020-00228-5
29. Raj DBTG, Khan NA (2016) Designer nanoparticle: nanobiotechnology tool for cell biology. Nano Converg 3(1):22.
https://doi.org/10.1186/s40580-016-0082-x
30. Azevedo-Pereira RL, Rangel B, Tovar-Moll F et al (2019) Superparamagnetic iron oxide nanoparticles as a tool to track mouse neural stem cells in vivo. Mol Biol Rep 46(1):191–198.
https://doi.org/10.1007/s11033-018-4460-9
31. Hu Y, Li D, Wei H et al (2021) Neurite extension and orientation of spiral ganglion neurons can be directed by superparamagnetic iron oxide nanoparticles in a magnetic field. Int J Nanomed 16:4515–4526.
https://doi.org/10.2147/ijn.s313673
32. Rampini S, Li P, Lee GU (2016) Micromagnet arrays enable precise manipulation of individual biological analyte-superparamagnetic bead complexes for separation and sensing. Lab Chip 16(19):3645–3663.
https://doi.org/10.1039/c6lc00707d
33. Jolivet JP, Chanéac C, Tronc E (2004) Iron oxide chemistry. From molecular clusters to extended solid networks. Chem Commun (5):481–487.
https://doi.org/10.1039/b304532n
34. Hiranuma M, Okuda Y, Fujii Y et al (2024) Characterization of human iPSC-derived sensory neurons and their functional assessment using multi electrode array. Sci Rep 14(1):6011.
https://doi.org/10.1038/s41598-024-55602-8
35. Yoshida S, Kato-Negishi M, Takeuchi S (2018) Assembly and connection of micropatterned single neurons for neuronal network formation. Micromachines 9(5):235.
https://doi.org/10.3390/mi9050235
36. Bakkum DJ, Frey U, Radivojevic M et al (2013) Tracking axonal action potential propagation on a high-density microelectrode array across hundreds of sites. Nat Commun 4:2181.
https://doi.org/10.1038/ncomms3181
37. Lee S, Kim S, Kim S et al (2018) A capsule-type microrobot with pick-and-drop motion for targeted drug and cell delivery. Adv Healthc Mater 7(9):e1700985.
https://doi.org/10.1002/adhm.201700985
38. Kim E, Jeon S, An HK et al (2020) A magnetically actuated microrobot for targeted neural cell delivery and selective connection of neural networks. Sci Adv 6(39):eabb5696.
https://doi.org/10.1126/sciadv.abb5696